



Soft Matter

New Approach for SANS Measurement of Micelle Chain Mixing During Size and Morphology Transitions

Journal:	<i>Soft Matter</i>
Manuscript ID	SM-ART-02-2023-000157.R1
Article Type:	Paper
Date Submitted by the Author:	06-Apr-2023
Complete List of Authors:	Larison, Taylor; University of South Carolina System, Chemistry and Biochemistry Pingali, Sai Venkatesh; Oak Ridge National Laboratory, Biology and Soft Matter Division Stefik, Morgan; University of South Carolina, Chemistry and Biochemistry; University of South Carolina

SCHOLARONE™
Manuscripts

New Approach for SANS Measurement of Micelle Chain Mixing During Size and Morphology Transitions

Taylor Larison,¹ Sai Venkatas Pingali,² and Morgan Stefik^{1*}

¹Department of Chemistry and Biochemistry, University of South Carolina, Columbia, South Carolina 29208, United States

²Neutron Scattering Division, Oak Ridge National Laboratory, Oak Ridge, Tennessee 37831, United States

*corresponding author e-mail: morgan@stefikgroup.com

Abstract

Chain exchange in amphiphilic block polymer micelles is measurable with time-resolved small-angle neutron scattering (TR-SANS) where contrast-matched conditions reveal chain mixing as reduced intensity. However, analyzing chain mixing on short time scales e.g. during micelle transformations remains challenging. SANS model fitting can quantify chain mixing during size and morphology changes, however short acquisition times lead to lower data statistics (higher error). Such data are unsuitable for form factor fitting, especially with polydisperse and/or multimodal scenarios. An integrated-reference approach, $R(t)$, is compatible with such data by using fixed reference patterns for the unmixed and fully mixed states that are each integrated to improve data statistics (lower error). Although the $R(t)$ approach is tolerant of low data statistics, it remains incompatible with size and morphology changes. A new shifting references relaxation approach, $SRR(t)$, is proposed where reference patterns are acquired at each time point to enable mixed state calculations regardless of short acquisition times. The additional experimental

measurements needed are described which provide these time-varying reference patterns. The use of reference patterns makes the $SRR(t)$ approach size/morphology-agnostic, allowing for the extent of micelle mixing to be directly calculated without this knowledge. $SRR(t)$ is thus compatible with arbitrary levels of complexity and can provide accurate assessment of the mixed state which could support future model analysis. Calculated scattering datasets were used to demonstrate the $SRR(t)$ approach during multiple size, morphology, and solvent conditions (Scenarios 1-3). The mixed state calculated from the $SRR(t)$ approach is shown to be accurate for all three scenarios.

Introduction

Block polymer micelles have applications that span from drug/gene delivery,¹⁻³ to nanoreactors,^{4,5} emulsions,⁶ and templates for nanomaterials.⁷⁻¹⁵ The characterization of how micelle size and morphology evolves over time as a result of chain mixing are important, but has remained elusive. Despite the capabilities of existing SANS models, there is not yet such an approach compatible with the low data statistics associated with rapid measurements during morphology/size transformations. This limitation has hampered analysis of chain exchange during morphology/size changes. Recent decades of research revealed much about chain exchange mechanisms and separately how size and morphology transitions evolve over time.¹⁶⁻²² For example, micelle morphology transitions have been induced by varying solvent or temperature conditions leading to mechanism insights for micelle fusion/fragmentation.²³⁻²⁸ However, these insights were generally restricted to ensemble rates of size/morphology change where the corresponding extent of chain mixing remained elusive. Time-resolved small-angle neutron scattering (TR-SANS) experiments are often used for measuring chain mixing due to the ability to control the source of signal intensity with isotope-labeled polymer chains (usually deuterated/protiated).^{19,23,37,29-36} Here contrast-matched conditions are generally used where the fully-mixed micelles (containing

equal moles of deuterated and protiated polymer) have the same scattering length density (SLD) as the solvent phase, thus giving the unmixed micelles the maximum scattered intensity. Separately, many studies have examined changes to micelle sizes, and morphology transitions either due to processes over time or as a result of thermodynamic changes (e.g. solvent composition changes).^{6,17,40–45,18–22,25,38,39} Here the “process time” is the duration of the chain exchange process which may be induced by e.g. quiescent sitting,^{30,46} stirring,²⁵ vortexing,³⁷ or ultrasonication.^{36,47} Often studies that emphasize size/morphology change rely upon measurements that are insensitive to chain mixing, e.g. small-angle X-ray scattering (SAXS) or transmission electron microscopy (TEM) due to the challenges of analyzing TR-SANS data with low signal statistics.

The analysis methods for deriving the extent of chain mixing from TR-SANS data can be grouped into two classes of approach: comprehensive form-factor models and form-factor-agnostic models. Here the form-factor is the scattering characteristic of an individual micelle which depends upon morphology, size, SLD differences (i.e. contrast) between all two-body pairs, and can include other contributions e.g. chain conformations. The addition of multiple distribution terms to these models as well as incoherent scattering bring additional complexity.^{34,48} There are numerous comprehensive SANS form-factor models for block polymer micelles that depend on the above factors.^{19,23,24,29,35,49–51} For example, the opensource SASfit program includes ~50 comprehensive micelle form-factor models (categories: spherical, ellipsoidal, cylindrical, rod-like, local planar).⁵² In principle, the use of such comprehensive form-factor models to fit data in units of absolute scattering intensity yields best-fit values for SLD which are simple to relate to the extent of chain mixing.^{34,35} The use of comprehensive models is most suitable for ideal datasets with long acquisition times and thus good data statistics. The derivation of a unique best-fit (as opposed to equivocal variations) is more challenging when there are wide/multi-modal size distributions or

morphology mixtures since the number of fit parameters increases. Compared to synchrotron X-ray sources, one inherent difficulty for SANS is acquiring sufficient data statistics on short time scales from the lower flux of neutron sources in order to resolve a meaningful form factor fit. Neutron sources typically have a flux on the order of $\sim 10^8$ neutrons/cm²s which is far lower than the $\sim 10^{12}$ - 10^{14} photons/s flux at synchrotron X-ray sources.³⁴ The brightness limitation of SANS instruments often require many minutes to hours of acquisition to have sufficient data statistics for robust form factor fitting.

Integrated-reference pattern approaches avoid the requirement for high-statistics $I(q)$ data by removing form-factor models and instead using reference datasets which are integrated over a range of q -space. Here the Poisson counting statistics is significantly improved by combining the counts from an ensemble of pixels thus yielding a higher statistics value as compared to the individual pixels. For example, the $R(t)$ relaxation function is often used to quantify the decrease in scattering intensity during chain mixing:^{19,23,37,29-36}

$$R(t) = \sqrt{\frac{I(t) - I(\infty)}{I(0) - I(\infty)}} \quad (\text{eq 1})$$

where $I(t)$ is the intensity at mixing time (t), $I(\infty)$ is the intensity of a fully-mixed sample prepared by premixing chains before micellization, and $I(0)$ is the intensity of the initial unmixed sample. Thus $I(0)$ and $I(\infty)$ set maximum and minimum anticipated scattering intensities. We note that these intensity values are often derived by integrating $I(q)$ over a q -range or alternatively by calculating $R(t, q)$ over a range of q -values and averaging them together with similar $R(t)$ results either way.^{29,33,36,37} Briefly it is also noted that the functional form of $R(t)$, with intensity differences calculated before taking the square root, enables the removal of scattering contributions that are unrelated to the mixing extent. The square root of the remaining scattered intensities relates

to the SLD-contrast of the present mixed state. It thus follows that the percent of chain mixing is $1-R(t)$ when a perfect contrast match is used. It should also be noted that the percent of chain mixing corresponds to the mixed state composition and is blind to mixing events that do not change the average composition, thus underestimating the total number of chain exchange events by at least a factor of two. For example, any micelle releasing a D-chain followed by insertion of a D-chain (constant aggregation number) does not result in a change of scattered intensity. This integral based approach is ideal for difficult to fit samples, such as those with significant dispersity. A drawback of the $R(t)$ approach, however, is that it assumes that all changes to intensity are related to chain mixing alone, which is only valid for size-invariant, morphology-invariant, and solvent-invariant experiments. For example, a recent study of chain mixing with the $R(t)$ method during size changes was limited to low-extents of mixing to avoid violating this assumption.³⁶ Herein a new analysis method is proposed where inclusion of shifting references relaxation function (SRR) enables chain mixing measurements with fast acquisitions (low data statistics) during morphology changes. Though motivated by micelles, this methodology applies equally well to diverse complex soft-matter systems including for example lipid exchange, surfactant exchange, emulsion oil exchange, or homopolymer exchange between micelles.

Results

The essential feature of the SRR approach is the inclusion of shifting (time-dependent) reference patterns for the mixed and unmixed states to account for variation of non-mixing related scattering

contributions such as size/morphology/solvent changes. Importantly, these shifting reference patterns are derivable directly from experimental measurements without knowledge of the micelle shape or size distributions, *vide infra*. This allows the $SRR(t)$ approach to measure chain mixing regardless of form-factor changes overtime. The $SRR(t)$ functional form is:

$$SRR(t) = \sqrt{\frac{I(t) - I_{pre-mixed}(t)}{I_{unmixed}(t) - I_{mixed}(t)}} \quad (\text{eq 2})$$

Here $I(t)$ corresponds to the measured sample undergoing chain mixing for a desired amount of time (t) and $I_{pre-mixed}(t)$ is a measured reference pattern for the fully-mixed condition. $I_{pre-mixed}(t)$ reference sample starts with pre-mixed H/D chains in micelles which undergo the same processing conditions over time. In this way, the $I_{unmixed}(t)$ reference reflects the non-mixing related intensity for the changing micelle size/morphology/solvents during the exchange process. This non-mixing related intensity is thus subtracted before comparing $I(t)$ to $I_{unmixed}(t)$ (eq 2). A unique feature for $SRR(t)$ is that the $I_{unmixed}(t)$ reference pattern is calculated from separate $I_H(t)$ and $I_D(t)$ measurements from purely H-labelled and D-labelled chains, separately (Figure 1). In this way the isotope-related contrast is maintained during size/morphology/solvent changes. Furthermore, since micelle chain exchange processes often depend on the chain concentration,^{25,36,37} each type of labelled chain must be measured with the same concentration as the rest of the samples (e.g. 1 wt% polymer for $I(t)$, $I_{pre-mixed}(t)$, $I_H(t)$, and $I_D(t)$). It follows then the sum of $I_H(t)$, and $I_D(t)$ will be twice that of the intended $I_{unmixed}(t)$ reference pattern (e.g. 1 wt%). Thus, their sum is halved which is equivalent to the average:

$$I_{unmixed}(t) = \frac{I_H(t) + I_D(t)}{2} \quad (\text{eq 3})$$

Please note that the $SRR(t)$ method is best suited for form factor patterns from dilute samples (<2 vol%) without structure factor contributions. Addressing more concentrated samples with Bragg scattering introduces additional complexity. Zero average contrast conditions do not yield structure

factor peaks as noted recently with experimental confirmation.⁵³ Thus additional modeling/fitting would be needed to remove the structure factor from the $I_H(t)$ and $I_D(t)$ measurements in order to calculate the corresponding $I_{\text{unmixed}}(t)$ without structure factor.

Figure 1 schematically shows how the necessary set of four scattering measurements ($I_H(t)$, $I_D(t)$, $I_{\text{pre-mixed}}(t)$, and $I(t)$) are combined for each $SRR(t)$ value. A constant background term was included for all Figure 1 calculations so that $I_{\text{pre-mixed}}(t)$ would have non-zero values to enable log-log plotting. An example sequence of measurements over time are depicted in Figure 2. The resulting $SRR(t)$ values are linear with mixing extent ($1-SRR(t)$) which multiplied by the concentration I yields the mixed chain concentration ($C*(1-SRR(t))$).^{36,37} To briefly summarize, $SRR(t)$ may be calculated from data that: 1) all undergo identical processing (temperature, agitation, etc.), 2) have identical concentration, and 3) are acquired with identical TR-SANS intervals or alternatively with arbitrary intervals when absolute scattering intensity is used (Figure 1,2). We note that time of flight detection is advantageous for flexible data re-binning where the four required scattering

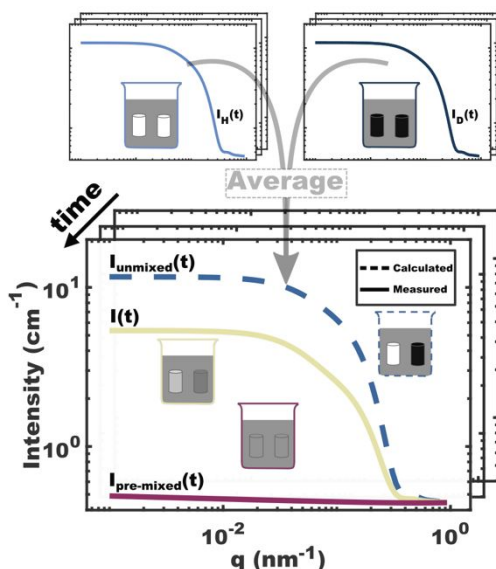


Figure 1: Schematic showing the data used for $SRR(t)$ calculation from accessible experimental measurements alone. This approach is compatible with arbitrary levels of complexity since it does not use an explicit form-factor model. Please note that these four measurements must be carried out in the same sequence of solvents with the same total polymer concentration, see text

patterns at each time point must be synchronized and with the same duration. For experiments

requiring very long durations, these four measurements could be run in parallel with staggered

start times. Such parallelization best fits with arrayed sample holders such that computer control

enables consistent process-time for each measurement. The implementation of $SRR(t)$ should also

consider experimental reproducibility, including e.g. temperature variation and concentration

error. Fortunately, these challenges have been widely addressed with prior approaches such as $R(t)$. In brief, active temperature control (Peltier or cartridge heater) with circulating medium can decouple sample temperature from ambient fluctuations. Likewise, concentration error can be minimized in experiment, design, e.g. by using stock solutions with large volumes. In the proceeding sections, simulated datasets are used to demonstrate the $SRR(t)$ approach for micelles during scenarios of size change (1S) and morphology change via solvent addition (2S). Crudely simple form factor models are used to calculate scattering curves for the sake of demonstration. Subsequent $SRR(t)$ calculations were carried out without using knowledge of the form factors, thus the approach remains form-factor agnostic and is compatible with arbitrary levels of size/morphology complexity. The final scenario (3S) follows a more comprehensive/realistic simulated dataset corresponding to a sequence including both morphology and size changes as inspired by recent data.²⁴

Time, t	$I_D(t)$	$I_H(t)$	$I_{unmixed}(t)$ *	$I(t)$	$I_{pre-mixed}(t)$
t_0					
t_1					
t_2					
t_∞					

Figure 2: Illustration showing the measurements needed ($I_D(t)$, $I_H(t)$, $I(t)$, $I_{pre-mixed}(t)$ and $I_{unmixed}(t)$) to calculate $SRR(t)$. *The unmixed reference pattern $I_{unmixed}(t)$ is calculated as the average of measured $I_D(t)$ and $I_H(t)$ patterns so that it has the same morphology distribution as $I(t)$, and $I_{unmixed}(t)$.

Following from the functional structure of $SRR(t)$, there are 4 empirical measurements needed for each timepoint evaluated (Figure 2). As with prior methods, an H- and D-labelled polymer chains are needed with equal moles. These are used to make three stock solutions: stock-1 containing equal moles of H- and D-labeled polymer chains at overall concentration C , for the $I_{pre-mixed}(t)$ data, stock-2 containing H-labeled polymer chains at concentration C for $I_H(t)$ and $I(t)$, and stock-3 containing D-labeled polymer chains at concentration C for $I_D(t)$ and $I(t)$. The $I(t)$ sample is prepared from equal volumes of stock-2 and stock-3 so that the overall concentration remains C . This criteria is important since a number of chain exchange processes are concentration dependent. Here the use of these additional reference patterns is the minimum information needed to use reference patterns for analysis with short acquisitions and low $I(q)$ statistics during morphology changes.

Before demonstrating SRR, however, the utility of integrated-reference approaches are first motivated with example SANS data. Spherical micelles (Figure S1) of ~ 17.6 kg/mol poly(ethylene oxide)-*b*-(methyl acrylate) (PEO-*b*-PMA) were measured to compare the error of the intensity with variable acquisition times. The data collected at the Bio-SANS instrument is stored with a time coordinate for every neutron measured which enables continuous acquisition data to be subsequently processed into arbitrary time intervals of the user's choice. Figures 3a and 3b shows the first 5 min interval (300s) and the first 1 min interval (60s) SANS data from a 60 min exposure. Changing the time interval from 300s to 60s results in a 5x lowering of the absolute count (Figure does not show absolute counts, it shows normalized counts). The main impact is seen in the intensity error where the error for the 60s sliced dataset ranged from 6-14%. With such low statistics (or large error bars), the form factor fitting approach becomes unreliable and, in many cases, infeasible. As noted earlier, counting statistics are significantly improved by combining the

counts of many detector pixels to increase the total number of counts. Thus, regardless of the $\sim 10\%$ point-by-point error in $I(q)$, the integral of the curve (I) had a significantly improved level of statistics with just a 3% propagated error. Regardless of the significant point-by-point error, both the 300s and 60s intervals yielded similar chain mixing trajectories (Fig. 3c). Thus, methods utilizing integrated data fundamentally enable shorter acquisition times which may be important to support studies of quick morphology transitions.

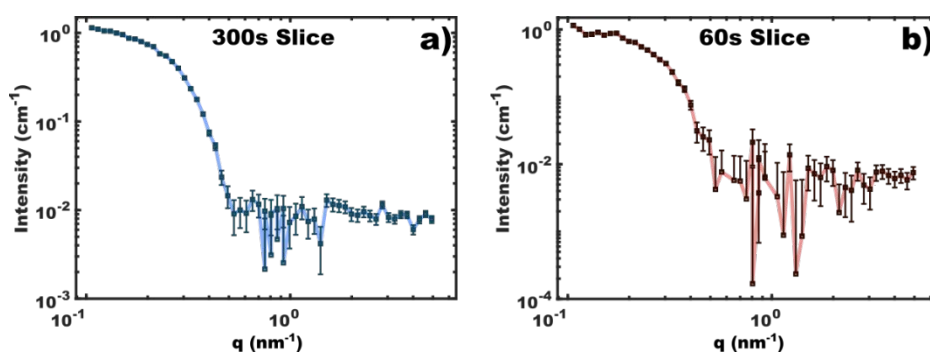


Figure 3: PEO-*b*-PMA micelle data collected at a concentration of 1 wt% polymer using SANS TOF with 300s (a), and 60s time intervals (b).

Simulated data sets are now used to demonstrate the capabilities and limitations of the $R(t)$ approach as a motivation for $SRR(t)$. For both $R(t)$ and $SRR(t)$ approaches, the use of mixed and unmixed reference scattering patterns is important, respectively, to subtract non-mixing related intensity and to calibrate the extent of mixing based on the unmixed reference. In this way, both $R(t)$ and $SRR(t)$ are form-factor-agnostic without need for explicit form-factor model(s). Two mixing scenarios were numerically simulated with SASfit. The first scenario (1S) included an abrupt size change (25-50 nm hard spheres) between the fourth- and fifth-time intervals. The second scenario (2S) included an abrupt morphology change (spheres-to-cylinders)^{54,55} between the fourth- and fifth-time intervals. This scenario (2S) also included a change of solvent, similar to a recent experimental example.¹⁹ Both scenarios used 10 time steps with a 10% increase in

mixed chain content at each time step. The parameters for simulation 1S are shown in Tables S5-S9 and those for 2S are shown in Tables S10-S14. The simulated mixing extent and size/morphology conditions are shown in Fig 4a and Fig 4d. For validation of interpretations, both $R(t)$ and $SRR(t)$ values are plotted with a second inverted y-axis so that the simulated extent of mixing is compared to the interpreted extent of mixing ($1-R(t)$ or $1-SRR(t)$). In this presentation format a valid interpretation (left y-axis) would align with the scenario conditions (right y-axis). Ideally the model interpretation corresponds closely to the input extent of mixing.

First the behavior of the $R(t)$ approach is examined with these two scenarios of simulated data. Figures 4b and 4e show $R(t)$ at each time step. For both scenarios, the implied extent of mixing ($1-R(t)$) accurately followed the simulated extent of mixing while the size/morphology was constant for time steps 1-4 (note alignment of $R(t)$ points with dotted line). Importantly, the extent of mixing does not follow the simulated extent of mixing when the size/morphology change occurs for time steps 5-10. For example, comparing the simulated extents of mixing to the implied extents of mixing ($1-R(t)$) leads to goodness-of-fit (R^2) values of 0.49 and 0.78, respectively. This inaccuracy arises since the $R(t)$ function uses two time-fixed reference patterns ($I(\infty)$ and $I(0)$) for all calculations which cannot address either changes to the non-mixing related intensity or the

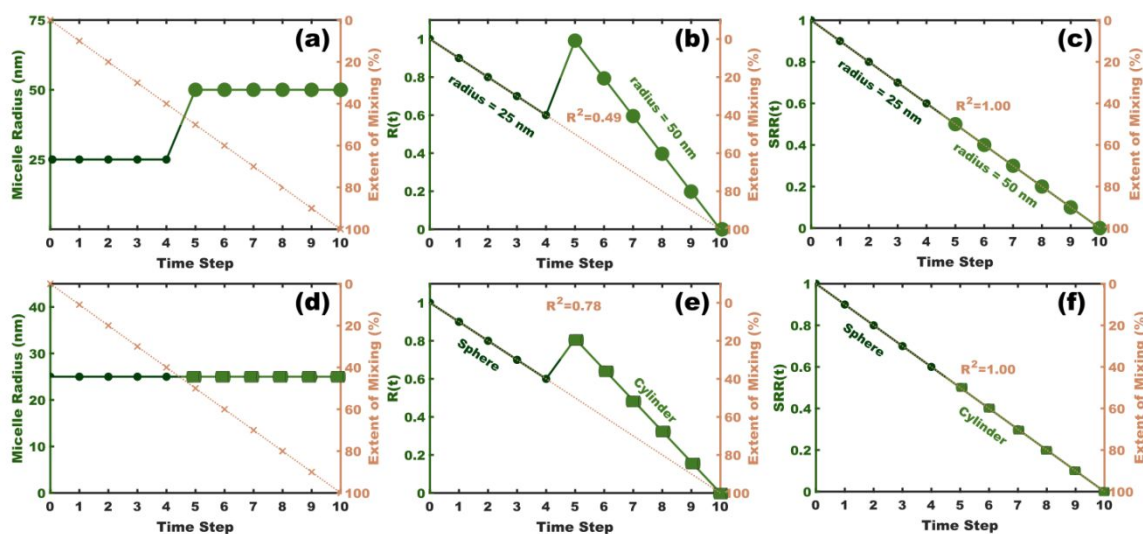


Figure 4: Capabilities and limitations of the $R(t)$ approach for simple scenarios 1S (top row) and 2S (bottom row). The first column corresponds to the simulated conditions (a, d). The second column corresponds to the $R(t)$ values (b, e) which imply inaccurate extents of mixing. The third column corresponds to the $SRR(t)$ values (c, f) which accurately determine the extent of mixing. Here the values on the two y-axes align when the model accurately predicts the extent of mixing. Goodness-of-fit R^2 values are presented.

changing scale of mixing-related intensity over time. The form-factor mismatch due to size/morphology/solvent change between $I(t)$ and $I(\infty)/I(0)$ are apparent for both scenarios at timestep 5 Fig S2a,b and Fig. S3a,b. Thus, the $R(t)$ approach is not suitable for tracking mixing processes with size/morphology/solvent changes.

The $SRR(t)$ method tracks chain exchange regardless of size/morphology changes by including shifting reference patterns for the unmixed and mixed states that are directly derived from experimental measurements (Fig 1, Fig 2). This approach is compatible with any non-mixing related scattering contributions that may occur and may vary with process time. The same two scenarios for micelle size and morphology changes (1S and 2S) were analyzed using SRR with simulated scattering curves. Here the time-dependent reference patterns allow the changes in non-mixing related intensity (changes in form factor) to be subtracted. For example, both scenarios have an abrupt change in form factor at time step 5. Here the shifting reference pattern for $I_{mixed}(t)$ and a calculated $I_{unmixed}(t)$ reference pattern have the same size/morphology as the sample, $I(t)$, since the measured micelles experience the same process time at the same concentrations. Thus, the intensity ratio (eq 2) purely corresponds to the extent of mixing. It is apparent that the implied extent of mixing ($1-SRR(t)$, Figure 4c,f) correctly follows the simulation input extent of mixing (Fig 4a,d) with goodness-of-fit R^2 values of 1.00. It is worth noting that simulation 2S also included terms to mimic a change of solvent composition. This solvent change leads to multiple changes to the scattering curve: the micelle-solvent contrast, the form factor, and the volume/number of micelles. Solvent composition changes are often used to induce micelle size/shape transitions where the ability to track chain exchange during such processes has remained challenging with

other methods. These simplified demonstrations with perfect contrast-matched conditions show that the SRR approach accurately extracts the extent of micelle mixing regardless of size/morphology/solvent changes.

Many micelle exchange experiments are conducted without a perfect contrast matched condition which is next considered. Often only one block of a polymer is deuterated for micelle mixing experiments due to the cost and complexity of isotope labelling. The third scenario (3S) includes non-perfect contrast-matched conditions (unlabeled micelle corona) that lead to additional non-mixing related scattering contributions. This scenario was inspired by recent experimental work²⁴ on cylindrical micelle fragmentation to spherical micelles followed by size equilibration (Figure 5a). In that study two pathways of micelle evolution were considered, both including initial fragmentation prior to the onset of chain mixing via single chain exchange. While form-factor observations were consistent with the preferred pathway, the lack of chain mixing characterization during this initial stage inhibits the consideration of alternative pathways. Validation of the chain mixing extent throughout the process is thus crucial when considering mechanisms of micelle evolution. Scenario 3S has a first fragmentation stage including gradual cylinder-to-sphere morphology change without chain mixing and the second equilibration stage including gradual size change with chain mixing (Figure 5a,b). Again, polymer volume was conserved throughout the simulated scattering curves. The simulated data for 3S show that the core-solvent contrast-match causes the expected intensity decay with increasing mixing extent, however the corona-core interface does not reach a contrast match upon mixing. Figure 5e shows the corresponding simulated scattering curves at time step 13 where the contribution of the corona SLD can be observed in the $I_{pre-mixed}(t)$ curve as it is above the background scattering. The resulting inclusion of these scattering contributions in $I(t)$ highlight the importance of removing their effects from

$SRR(t)$ by including time-dependent $I_{pre-mixed}(t)$ measurements. A complete list of the 3S form factor models and simulation parameters used are in tables S15-S18. The $R(t)$ approach was used to analyze dataset 3S (Figure 5c). As expected for morphology/size changes, the implied extent of mixing ($1-R(t)$) poorly matched the simulated extent of mixing with a goodness-of-fit R^2 value of -0.085. The $SRR(t)$ approach was also used to analyze dataset 3S (Figure 5d) with shifting reference patterns to account for the changing morphology/size distribution at each time step (Fig. 5d). In contrast, the implied extent of mixing ($1-SRR(t)$) closely tracked the simulated extent of mixing with a goodness of fit $R^2=0.99$ despite the lack of perfect contrast-matched conditions. The capability to track chain mixing during dynamic micelle size/morphology changes is thus

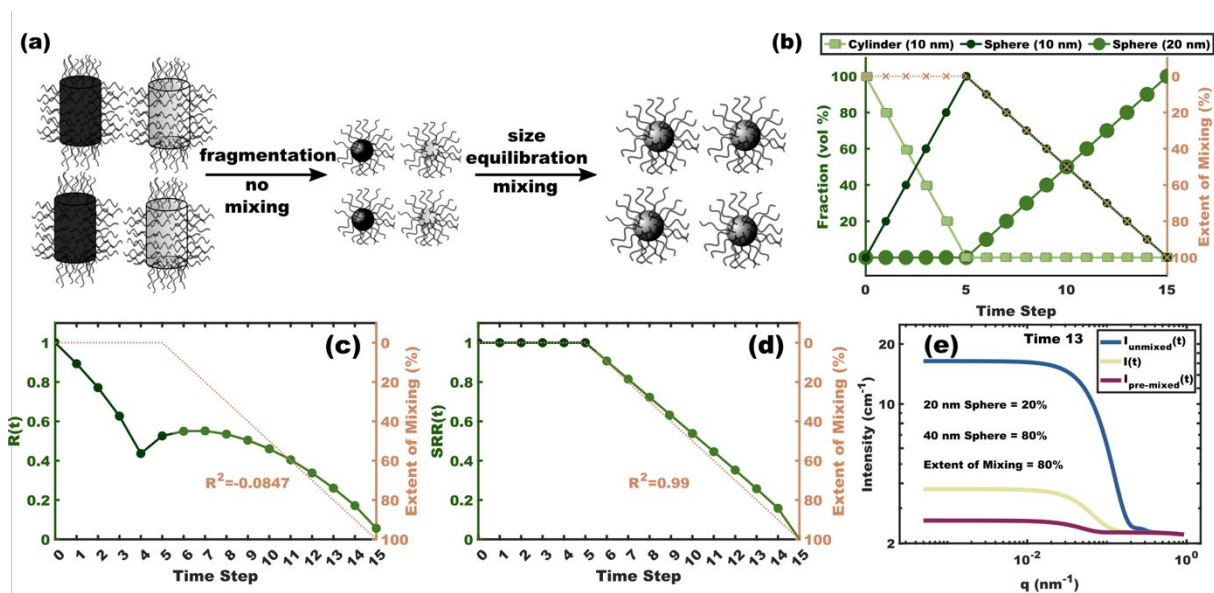


Figure 5: $SRR(t)$ was applied to a complex scenario (3S) without a perfect contrast-match. The sequence of morphology and size changes are depicted (a) and presented as a plot (b). The corresponding $R(t)$ values (c) and $SRR(t)$ values (d) are shown. Here the values on the two y-axes align when the interpretation is correct and the R^2 values corresponds to the goodness-of-fit. Example scattering curves are presented that include non-mixing related contrast (e).

thoroughly shown with dataset 3S. The ability to track micelle chain exchange during such dynamic environments with $SRR(t)$ will enable new insights to better support micelle evolution mechanisms that have previously been difficult to fully characterize.

Conclusion

The measurement of micelle chain mixing is important for understanding micelle evolution mechanisms over time. Explicit form-factor fitting is powerful but can be non-feasible while measuring weakly scattering micellar systems that quickly change. The well-known $R(t)$ approach is compatible with shorter acquisition times but is limited to systems which preserve constant size/morphology/solvent due to the use of fixed reference patterns. This work demonstrates a new $SRR(t)$ approach that calculates the extent of chain mixing by including time-varying reference patterns to account for non-mixing related scattering variations such as morphology/size changes. These reference patterns are all obtainable from convenient experimental measurements as described in Figures 1 and 2. Simulated datasets demonstrated the advantages of $SRR(t)$ with simplified scenarios including size change (1S) and morphology/solvent change (2S) with perfect contrast-match. Furthermore, a comprehensive scenario (3S) of a cylinder-to-sphere transition followed by size equilibration were simulated with more typical, non-perfect contrast-match conditions (unlabeled corona). Again $SRR(t)$ analysis accurately tracked the extent of micelle chain mixing. Future experimental implementation of the $SRR(t)$ approach would enable access to micelle chain mixing kinetics during dynamic processes which are important for mechanism determination.

Methods

All simulated scattering curves were generated using SASfit version 0.94.11 Darwin_x86_64. The q -range selected for simulated data was from $5 \cdot 10^{-4}$ - 1.0 nm^{-1} with a resolution of 100 points. All

calculated patterns included constant background such that all datasets were non-zero and thus plottable on log-log graphs. The SASfit “background” function was used for Figure 1 and Scenarios 1S and 2S with $C_0=1e-5$, $C_1=1e-5$, $C_4=1e-3$, and $\text{Alpha}=1e-5$ where the background intensity is $C_0+C_1*q+C_4*q^{-\text{Alpha}}$.

Simulated Size Change Data Set 1 (1S):

The first data set used the hard sphere form factor (“sphere”) with a gaussian distribution of sphere radii. A background was included to mimic generic background scattering from solvent. The complete list of parameter values are presented in Tables S1-S2. The scattering contrast (η) values were decreased linearly with 10 time steps. As noted elsewhere with agitation induced exchange and cavitation induced exchange^{25,36}, these simulations included a sudden micelle size change between the 4th and 5th time step. Simultaneously, the particle number density (N) was changed from $1.0e-30$ to $1.25e-31$ to conserve polymer volume. The particle percent dispersity ($S/\text{radius}(XO)$) was also conserved.

Simulated Morphology Change Data Set 2 (2S):

The second data set used hard sphere and hard cylinder (“cylinder”) form factors, similar to dataset 1S. A full list of the simulation parameters are in Tables S3-S5.

Simulated Transition Experiment (non-contrast matched chains) Data Set 3 (3S):

The third data set used a core-shell cylindrical and core-shell spherical form factor (“CYL+Chains(RW)_Rc”, “BlockCopolymerMicelle”) in SASfit^{52,56} with a gaussian distribution of the core radius and a gaussian distribution of the aggregation number respectively. Simulations

mimicked a three-part process: 1) fragmentation of cylinders into small spheres, 2) transition of small spheres into larger spheres, 3) mixing of micelles during sphere-to-sphere transition (Fig. 3a). A list of parameters can be found in table S6-S9.

Calculations

The time-dependent eta terms for SLD contrast were varied over time where:

$$\%mixed = \frac{\eta(t) - \eta(\infty)}{\eta(0) - \eta(\infty)} * 100\% \quad (\text{eq 4})$$

The R(t) values were calculated using eq. 1 from the integrated intensity of the simulated scattering curves across the full simulated q-range. The SRR(t) values were calculated analogously using eq. 4 with the exception that $I_{unmixed}(t)$ was calculated from separate $I_H(t)$ and $I_D(t)$ scattering curves as would be done with experimental data using eq. 3.

Materials: Poly(ethylene glycol) methyl ether (PEO-OH, Mn = 5,000 g mol⁻¹, Aldrich), 2-bromopropionic acid (>99%, Aldrich), and 4-(dimethylamino)pyridine (99%, Aldrich), N,N'-dicyclohexylcarbodiimide (DCC) (99%, BeanTown Chemical), 4-dimethylaminopyridine (DMAP) (99%, TCI Chemicals), acryloyl chloride (96%, stabilized with 400 ppm phenothiazine, Alfa Aesar), 4-methoxyphenol (99%, Acros Organics), triethylamine (>99.5% Millipore Sigma), dimethylformamide (97%, Aldrich) were used as received. The catalyst, copper(I) bromide (99.99%, Aldrich), ligand, tris[2-(dimethylamino)ethyl]amine (97%, Aldrich), and anhydrous, inhibitor-free tetrahydrofuran (THF, 99% Aldrich) were stored inside a glovebox and used as received. Methanol (MeOH, 99.8%, Fisher) was dried at room temperature by storage over 30% w/v of molecular sieves (3 Å, 8–12 mesh, Acros Organics) for a week. Deuterium oxide (D2O, 99.9% D) was purchased from Cambridge Isotopes and used as received. Deuterated Methanol

(MeOD, 99.9% D₄) was purchased from Cambridge Isotopes and used as received. Methyl acrylate (99%, stabilized) was run over an alumina column prior to use. All reagents were used as received without any further purification unless otherwise stated.

Poly(ethylene oxide) Macro-Initiator Synthesis:

PEO-Br was synthesized via a Steglich esterification. Poly(ethylene glycol) monomethyl ether with a molecular weight of 5,000 g/mol (20 g, 4.0 mmol) was dissolved in 100 mL of chloroform. Next, 2-bromopropionic acid (0.720 mL 8.00 mmol) was added dropwise while stirring. The solution was brought to 0°C for 10 minutes prior to the addition of N,N'-dicyclohexylcarbodiimide (DCC) (1.65 g 8.0 mmol) and 4-dimethylaminopyridine (DMAP) (0.391 g 3.20 mmol). The suspension was then allowed to stir for 2 hours at 0°C for 2 hours, brought to room temperature and allowed to stir overnight. The crude product was isolated via vacuum filtration to remove the urea by-product. The filtrate was then added to hexane (1000 mL) to isolate PEO-Br macroinitiator. The precipitant was collected via vacuum filtration and allowed to dry in a vacuum chamber overnight. The final product was collected for an 87% yield as verified with ¹H-NMR.

Poly(ethylene oxide-*b*-methyl acrylate) Synthesis:

Previously synthesized PEO-Br (1 g, 0.2 mmol), and methyl acrylate (4.216 g, 49 mmol) was dispersed in 1 mL of anisole. The solution was treated to 3 cycles of freeze-pump-thaw to remove oxygen and brought into an argon glovebox. A copper stock solution of copper(I) bromide (35.86 mg, 0.25 mmol) Me₆TREN (66.81 mL, 57.6 mg, 0.25 mmol) was dispersed in 0.5 mL of toluene. To the PEO-Br, MA solution 0.2 mL of copper stock solution was added. The solution was then

placed in a preheated oil bath at 80°C and stirred for 16 hours. The final product was collected by precipitation in methanol and dried in a vacuum chamber overnight. The final product was validated with $^1\text{H-NMR}$.

SANS Measurements:

SANS measurements were performed on the CG-3 Bio-SANS instrument at the High Flux Isotope Reactor at Oak Ridge National Laboratory.^{57,58} Sample preparation was carried out by generating micelle solutions. The solutions were made by dispersing the polymer in methanol at a concentration of 10 wt% followed by the addition of a $\text{H}_2\text{O}/\text{D}_2\text{O}$ (77.16/22.84 vol%) mixture until the solution was 50/50 (vol%) $\text{MeOH}/(\text{H}_2\text{O}/\text{D}_2\text{O})$. The polymer was then diluted with a solution of 50/50 (vol%) $\text{MeOH}/(\text{H}_2\text{O}/\text{D}_2\text{O})$ until a final concentration of 1 wt% was achieved. A volume of 0.35 mL of the final solution was added into a titanium cell for SANS measurements. The nominal neutron wavelength was 0.6 nm with a detected q -range spanning from 0.007-9.25 nm^{-1} .

ASSOCIATED CONTENT

Supporting Information

See Supplemental Material at [URL from publisher] for materials, experimental procedures, calculations, simulations, and parameters, SANS scattering curves, and DLS data

AUTHOR INFORMATION

Corresponding Author

Morgan Stefik – *Department of Chemistry and Biochemistry, University of South Carolina, Columbia, South Carolina 29208, United States*; Present Address: Department of Chemistry and Biochemistry, University of South Carolina, Columbia, South Carolina 29208, United States; orcid.org/0000-0002-2645-7442; Email: morgan@stefikgroup.com

Author Contributions

The manuscript was written through contributions of all authors. / All authors have given approval to the final version of the manuscript.

Funding Sources

NSF Award #DMR-1752615

ACKNOWLEDGMENT

T.L. and M.S acknowledge support by a National Science Foundation under NSF Award #DMR-1752615. M.S. acknowledges support by the Hanse-Wissenschaftskolleg Institute for Advanced Study, Delmenhorst, Germany. Neutron scattering research conducted at the Bio-SANS instrument, a DOE Office of Science, Office of Biological and Environmental Research resource (FWP ERKP291), used resources at the High Flux Isotope Reactor, a DOE Office of Science, Scientific User Facility operated by the Oak Ridge National Laboratory. Oak Ridge National Laboratory is managed by UT-Battelle, LLC, for the U.S. Department of Energy under Contract DE-AC05-00OR22725. This manuscript has been coauthored by UT-Battelle, LLC, under Contract No. DE-AC05-00OR22725 with the U.S. Department of Energy. The United States Government retains and the publisher, by accepting the article for publication, acknowledges that the United States Government retains a nonexclusive, paid-up, irrevocable, worldwide license to publish or reproduce the published form of this manuscript, or allow others to do so, for United States Government purposes. The Department of Energy will provide public access to these results of federally sponsored research in accordance with the DOE Public Access Plan (<http://energy.gov/downloads/doe-public-access-plan>).

References

- 1 H. Cabral, K. Miyata, K. Osada and K. Kataoka, *Chem. Rev.*, 2018, 118, 6844–6892.
- 2 N. Nishiyama and K. Kataoka, *Pharmacol. Ther.*, 2006, **112**, 630–648.
- 3 K. Kataoka, A. Harada and Y. Nagasaki, *Adv. Drug Deliv. Rev.*, 2012, **64**, 37–48.
- 4 R. Kaur and P. Khullar, *Mater. Biomed. Eng. Inorg. Micro- Nanostructures*, 2019, 177–210.
- 5 Y. Liu, Y. Wang, Y. Wang, J. Lu, V. Piñón and M. Weck, *J. Am. Chem. Soc.*, 2011, **133**, 14260–14263.
- 6 P. Alexandridis and T. Alan Hatton, *Colloids Surfaces A Physicochem. Eng. Asp.*, 1995, **96**, 1–46.
- 7 M. Templin, A. Franck, A. Du Chesne, H. Leist, Y. Zhang, R. Ulrich, V. Schädler and U. Wiesner, *Science (80-.)*, 1997, **278**, 1795–1798.
- 8 D. Zhao, J. Feng, Q. Huo, N. Melosh, G. H. Fredrickson, B. F. Chmelka and G. D. Stucky, *Science*, 1998, **279**, 548–552.
- 9 V. N. Urade and H. W. Hillhouse, *J. Phys. Chem. B*, 2005, **109**, 10538–10541.
- 10 S. C. Warren, L. C. Messina, L. S. Slaughter, M. Kamperman, Q. Zhou, S. M. Gruner, F.

- J. DiSalvo and U. Wiesner, *Science*, 2008, **320**, 1748–1752.
- 11 J. Bolton, T. S. Bailey and J. Rzyayev, *Nano Lett.*, 2011, 998–1001.
- 12 K. Peters, H. N. Lokupitiya, D. Sarauli, M. Labs, M. Pribil, J. Rathouský, A. Kuhn, D. Leister, M. Stefik and D. Fattakhova-Rohlfing, *Adv. Funct. Mater.*, 2016, **26**, 6682–6692.
- 13 K. A. Lantz, N. B. Clamp, W. van den Bergh, A. Sarkar and M. Stefik, *Small*, 2019, **15**, 1–10.
- 14 W. van den Bergh, H. N. Lokupitiya, N. A. Vest, B. Reid, S. Guldin and M. Stefik, *Adv. Funct. Mater.*, 2021, **31**, 1–11.
- 15 E. R. Williams, P. L. McMahon, J. E. Reynolds, J. L. Snider, V. Stavila, M. D. Allendorf and M. Stefik, *Mater. Adv.*, 2021, **2**, 5381–5395.
- 16 A. Halperin and S. Alexander, *Macromolecules*, 1989, **22**, 2403–2412.
- 17 P. Alexandridis and R. J. Spontak, *Curr. Opin. Colloid Interface Sci.*, 1999, **4**, 130–139.
- 18 L. Luo and A. Eisenberg, *Langmuir*, 2001, **17**, 6804–6811.
- 19 R. Lund, V. Pipich, L. Willner, A. Radulescu, J. Colmenero and D. Richter, *Soft Matter*, 2011, **7**, 1491–1500.
- 20 M. S. Hsiao, S. F. M. Yusoff, M. A. Winnik and I. Manners, *Macromolecules*, 2014, **47**, 2361–2372.
- 21 K. A. Dill, S. Bromberg and D. Stigter, *Polymer Solutions*, 2018, vol. 3.
- 22 L. Kumar, A. Horechyy, E. Bittrich, B. Nandan, P. Uhlmann and A. Fery, *Polymers (Basel)*, , DOI:10.3390/polym11111882.
- 23 R. Lund, L. Willner, V. Pipich, I. Grillo, P. Lindner, J. Colmenero and D. Richter, *Macromolecules*, 2011, **44**, 6145–6154.
- 24 R. Lund, L. Willner, D. Richter, P. Lindner and T. Narayanan, *ACS Macro Lett.*, 2013, **2**, 1082–1087.
- 25 E. G. Kelley, R. P. Murphy, J. E. Seppala, T. P. Smart, S. D. Hann, M. O. Sullivan and T. H. Epps, *Nat. Commun.*, 2014, **5**, 3599.
- 26 D. Zhao, E. Wang and T. P. Lodge, *Macromolecules*, 2020, **53**, 7705–7716.
- 27 J. T. Early, A. Block, K. G. Yager and T. P. Lodge, *J. Am. Chem. Soc.*, 2021, **143**, 7748–7758.
- 28 C. C. M. Sproncken, J. R. Magana and I. K. Voets, *ACS Macro Lett.*, 2021, **10**, 167–179.
- 29 L. Willner, A. Poppe, J. Allgaier, M. Monkenbusch and D. Richter, *Europhys. Lett.*, 2001, **55**, 667–673.
- 30 R. Lund, L. Willner, D. Richter and E. E. Dormidontova, *Macromolecules*, 2006, **39**, 4566–4575.
- 31 R. Lund, L. Willner, J. Stellbrink, P. Lindner and D. Richter, *Phys. Rev. Lett.*, 2006, **96**, 1–4.
- 32 S. H. Choi, T. P. Lodge and F. S. Bates, *Phys. Rev. Lett.*, 2010, **104**, 1–4.
- 33 J. Lu, S. Choi, F. S. Bates and T. P. Lodge, *ACS Macro Lett.*, 2012, **1**, 982–985.
- 34 R. Lund, L. Willner and D. Richter, in *Controlled Polymerization and Polymeric Structures*, Springer International Publishing: New York, 2013, vol. 259, pp. 51–158.
- 35 T. Zinn, L. Willner, R. Lund, V. Pipich and D. Richter, *Soft Matter*, 2012, **8**, 623–626.
- 36 K. A. Lantz, A. Sarkar, K. C. Littrell, T. Li, K. Hong and M. Stefik, *Macromolecules*, 2018, **51**, 6967–6975.
- 37 R. P. Murphy, E. G. Kelley, S. A. Rogers, M. O. Sullivan and T. H. Epps, *ACS Macro Lett.*, 2014, **3**, 1106–1111.
- 38 E. E. Dormidontova, *Macromolecules*, 1999, **32**, 7630–7644.

- 39 C. M. Bates and F. S. Bates, *Macromolecules*, 2017, **50**, 3–22.
- 40 J. A. Zupancich and F. S. Bates, 2006, **14**, 4286–4288.
- 41 S. Choi, F. S. Bates and T. P. Lodge, 2009, 13840–13848.
- 42 L. Yin and M. A. Hillmyer, *Macromolecules*, 2011, **44**, 3021–3028.
- 43 L. Yin, T. P. Lodge and M. A. Hillmyer, 2012, 1–8.
- 44 A. O. Moughton, M. A. Hillmyer and T. P. Lodge, *Macromolecules*, 2012, **45**, 2–19.
- 45 S. H. Choi, F. S. Bates and T. P. Lodge, *Macromolecules*, 2014, **47**, 7978–7986.
- 46 Y. Y. Won, H. T. Davis and F. S. Bates, *Macromolecules*, 2003, **36**, 953–955.
- 47 H. N. Lokupitiya and M. Stefik, *Nanoscale*, 2017, **9**, 1393–1397.
- 48 J. S. Pedersen, in *Soft Matter Characterization*, eds. R. Borsali and R. Pecora, Springer International Publishing, 2008, pp. 191–234.
- 49 R. Lund, L. Willner and D. Richter, in *Controlled Polymerization and Polymeric Structures: Flow Microreactor Polymerization, Micelles Kinetics, Polypeptide Ordering, Light Emitting Nanostructures*, eds. A. Abe, K.-S. Lee, L. Leibler and S. Kobayashi, Springer International Publishing, Cham, 2013, pp. 51–158.
- 50 T. Narayanan, H. Wacklin, O. Konovalov and R. Lund, *Crystallogr. Rev.*, 2017, **23**, 160–226.
- 51 J. E. Nielsen and R. Lund, *Langmuir*, 2022, **38**, 374–384.
- 52 J. Kohlbrecher, *Internet*, 2019, 688.
- 53 S. H. Choi, F. S. Bates and T. P. Lodge, *Macromolecules*, 2011, **44**, 3594–3604.
- 54 Lord Rayleigh, *Proc. R. Soc. A Math. ical, Phys. Eng. Sci.*, 1914, **90**, 324–328.
- 55 G. Porod, *Acta Phys. Austriaca*, 1948, **2**, 255–292.
- 56 J. S. Pedersen and M. C. Gerstenberg, *Macromolecules*, 1996, **29**, 1363–1365.
- 57 W. T. Heller, V. S. Urban, G. W. Lynn, K. L. Weiss, H. M. O’Neill, S. V. Pingali, S. Qian, K. C. Littrell, Y. B. Melnichenko, M. V. Buchanan, D. L. Selby, G. D. Wignall, P. D. Butler and D. A. Myles, *J. Appl. Crystallogr.*, 2014, **47**, 1238–1246.
- 58 W. T. Heller, M. Cuneo, L. Debeer-Schmitt, C. Do, L. He, L. Heroux, K. Littrell, S. V. Pingali, S. Qian, C. Stanley, V. S. Urban, B. Wu and W. Bras, *J. Appl. Crystallogr.*, 2018, **51**, 242–248.